Alignment and orientation in He 21P and 31P excitation by electron impact

Article *in* Journal of Physics B Atomic and Molecular Physics · January 1999

DOI: 10.1088/0022-3700/20/1/019

D. H. Madison
Missouri University of Science and Technology

Alignment and orientation in He 2^1P and 3^1P excitation by electron impact

1987 J. Phys. B: At. Mol. Phys. 20 167

(http://iopscience.iop.org/0022-3700/20/1/019)

J. Phys. B: At. Mol. Phys. **20** (1987) 167-181. Printed in the UK

Alignment and orientation in He 2^1P and 3^1P excitation by electron impact

J P M Beijers†, D H Madison‡, J van Eck† and H G M Heideman†

† Fysisch Laboratorium, Rijksuniversiteit Utrecht, Princetonplein 5, 3584 CC Utrecht, The Netherlands

‡ Physics Department, Drake University, Des Moines, Iowa 50311, USA

Received 16 May 1986

Abstract. We have studied the orientation and alignment of the 2^1P and 3^1P states of helium caused by electron impact at incident energies between 50 and 80 eV both experimentally and theoretically as a function of the electron scattering angle. The angular correlations between inelastically scattered electrons and VUV de-excitation photons were measured, particularly in the region where the orientation changes sign. The experimental results were compared with several distorted-wave models. The best of these models gave reasonably good agreement with the experimental data for excitation of the 2^1P and 3^1P states for scattering angles of less than 60° and qualitative agreement for larger angles.

1. Introduction

Since the introduction of electron-photon coincidence experiments in atomic physics by Eminyan *et al* (1973, 1974), the technique has been used by many groups to obtain very detailed scattering information on electron-atom collisions. Because of the planar symmetry in this type of experiment, a considerable amount of orientation of the target atom can be produced. This provides a sensitive probe of the electron-atom interaction, unattainable in the more conventional type of cross section experiment. This more detailed information originates from the coincident detection of the inelastically scattered electron and the accompanying decay photon. In this manner both the magnitudes and the phases of the different scattering amplitudes or, equivalently, the orientation and alignment parameters of the excited target can be determined without the necessity to sum or integrate over unobserved variables (except for the spin). As a result, a very detailed test of the various theoretical models is made possible. For further information the reader is referred to one of the recent review articles (Blum and Kleinpoppen 1979, Slevin 1984).

Most experiments until now have been performed on the 2^1P state of helium (Eminyan *et al* 1974, Crowe *et al* 1983, Neill and Crowe 1984, Hollywood *et al* 1979, McAdams *et al* 1980, Slevin *et al* 1980, Steph and Golden 1980, van Linden van den Heuvell *et al* 1982) at collision energies ranging from the excitation threshold to several hundred eV. As a result, we have a reasonably well established knowledge of the behaviour of the coincidence parameters as a function of scattering angle and energy for this collision system. On the theoretical side, several models have been developed. In the low-energy region (up to a few eV above threshold) the R-matrix theory gives good results (Fon *et al* 1980) especially for energies below the 3^1P threshold (Crowe *et al* 1983). For higher energies, perturbative methods are usually used to calculate the differential cross sections and coincidence parameters (see, for example, the recent review of Walters (1984)). In this higher-energy region the theoretical models do not agree as well with the experimental data as those for the lower energies, although the qualitative features are reproduced. Much less work has been done on the higher excited states of helium. Eminyan *et al* (1975) and McAdams and Williams (1982) measured angular correlations for the 3^1P state of helium, while Standage and Kleinpoppen (1976) performed a complete Stokes' parameter analysis of the $3^1P \to 2^1S$ coincident photons. All these experiments were performed at 80 eV incident electron energy. By detecting the VUV photons resulting from the $3^1D \to 2^1P \to 1^1S$ cascade, van Linden van den Heuvell *et al* (1981, 1983) obtained information about the 3^1D scattering amplitudes at a fixed scattering angle for incident electron energies between 28 and 45 eV. Some work has also been done for the heavier rare gases (King *et al* 1985, Danjo *et al* 1985). These experiments are of special significance since they provide a probe of the spin-orbit interaction without using spin-polarised electrons or targets.

The excitation of the 2^1P state of helium is the only process that has been extensively investigated with coincidence techniques. However, despite these experimental and theoretical efforts, no clear physical picture of the interaction process existed until recently. In this work we present results of electron-photon coincidence experiments for the 2^1P and 3^1P excitation of helium at incident electron energies of 50, 60 and 80 eV. These states were studied by observing the VUV photons which resulted from the decay to the 1^1S ground state. Systematic measurements were made for scattering angles ranging from 25 to 90°. The results are presented in terms of the angular momentum transferred to the atom and the alignment angle of the charge cloud in the scattering plane. The present experimental results are compared with previous experiments and the results of several distorted-wave models. The necessary theory is briefly summarised in § 2. The experimental apparatus and measuring procedure are described in § 3 and the results and conclusions are presented in § 4. SI units are used throughout.

2. Theory

2.1. Angular correlation parameters

The theory of electron-photon coincidence experiments relating the observed angular or polarisation distribution of coincident photons to a set of parameters which describe the excited state under consideration is well known and can be found, for example, in Macek and Jaecks (1971), Fano and Macek (1973), Blum and Kleinpoppen (1975) and Nienhuis (1980). Depending on the chosen quantisation axis, the scattering amplitudes of the excited ^{1}P state are either parametrised with the so-called λ, χ parameters (quantisation axis parallel to the electron beam axis) or the μ, η parameters (quantisation axis perpendicular to the scattering plane). Although these two sets of parameters are formally equivalent, the μ, η parameters have recently been receiving more attention because of their physical significance (Hermann and Hertel 1982). The μ parameter is equal to the expectation value of the angular momentum transferred to the atom and the η parameter gives the alignment angle of the excited-electron cloud (see Andersen *et al* 1985). In the present work we use this parametrisation. For convenience we briefly describe the theory here.

Firstly we assume that all spin-dependent interactions can be neglected, so that only the orbital system need be considered. Atomic states are characterised accordingly in the LS coupling scheme. We use a right-handed coordinate system, with the xy plane as the scattering plane and the incoming electron beam parallel to the x axis. The quantisation axis (z axis) is perpendicular to the scattering plane (see figure 1).

By detecting the scattered electrons, which are energy analysed, in coincidence with the de-excitation photons, a subensemble consisting of atoms all excited in exactly the same way is prepared. Since the initial state is a pure state and no averaging over unobserved variables has to be performed (spin is neglected), the excited state is also a pure state and can be described by a single state vector

$$|\psi(^1\mathrm{P})\rangle = \sum_M a_M(\theta_e, E)|LM\rangle \tag{1}$$

i.e. as a superposition of magnetic substates $|LM\rangle$ of the ^{1}P state ($L=1$). The scattering amplitudes a_M are still functions of the scattering angle θ_e and the incident electron energy E. Because of reflection symmetry with respect to the scattering plane, the $|10\rangle$ magnetic substate cannot be excited, so $a_0 = 0$. Remember that this is only true when spin–orbit forces can be neglected. Indeed, for the heavier rare gases, 'out of plane' excitation is a sensitive probe of the strength of the spin–orbit coupling. The scattering amplitudes a_1 and a_{-1} can be parametrised by three real parameters, σ, μ and η, defined by

$$\sigma = |a_1|^2 + |a_{-1}|^2 \qquad \mu = \frac{|a_1|^2 - |a_{-1}|^2}{|a_1|^2 + |a_{-1}|^2} \qquad \eta = \arg\left(\frac{a_{-1}}{a_1}\right). \tag{2}$$

The parameter σ is the differential excitation cross section, μ is equal to the expectation value of the orbital angular momentum $L_\perp$ transferred to the atom during the collision and η is the phase difference between a_{-1} and a_1. In order to relate σ, μ and η to parameters which describe the excited-state charge cloud, we calculate the charge cloud density in the scattering plane. From equations (1) and (2) we obtain

$$|\psi|^2 \sim 1 - (1-\mu^2)^{1/2}\cos(2\varphi - \eta) = 1 + P_l \cos 2(\varphi - \gamma) \tag{3}$$

with

$$\begin{aligned} P_l &= (1-\mu^2)^{1/2} \\ \gamma &= \tfrac{1}{2}(\eta + \pi). \end{aligned} \tag{4}$$

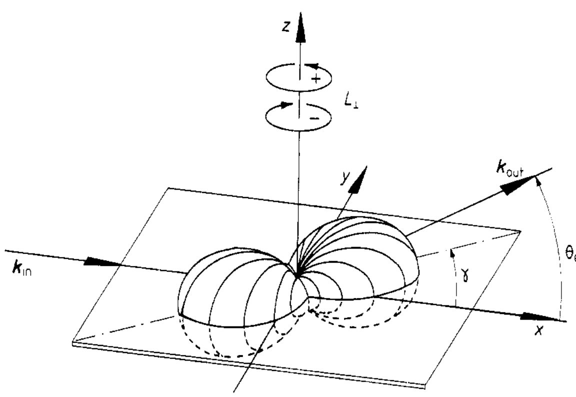

Figure 1. Definition of the coordinate system. The incoming electrons, parallel to the x axis, are scattered through an angle θ_e in the xy scattering plane. The alignment angle of the excited-electron cloud is designated by γ. The transferred angular momentum $L_\perp$ is parallel to the z axis.

Here φ is the angular coordinate of the scattering-plane charge distribution measured relative to the x axis. The parameter P_l is a width parameter and γ is the alignment angle of the charge cloud density in the scattering plane (Andersen *et al* 1985), cf figure 2. When $P_l = 1$ the angular momentum transfer $L_\perp = 0$ and a pure P orbital is excited.

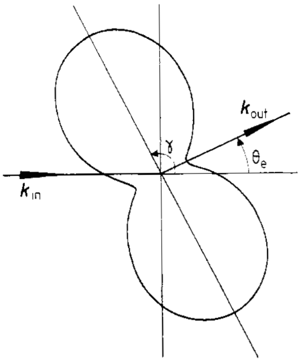

Figure 2. Charge-cloud density in the scattering plane for a 2^1P state excited by 80 eV electrons which are scattered through an angle $\theta_e = 25°$. The charge cloud is characterised by a width parameter $P_l = 0.69$ and an alignment angle $\gamma = 117°$.

The anisotropy of the excited ^{1}P state is reflected in the anisotropy of the de-excitation radiation. Thus, by measuring the angular correlation or polarisation correlation of the coincident de-excitation photons, the μ, η parameters can be determined. To determine these correlation functions we introduce the density operator ρ_u of the excited ^{1}P state:

$$\rho_u = |\psi\rangle\langle\psi| = \sum_{M,M'} |1M\rangle a_M a^*_{M'} \langle 1M'|. \tag{5}$$

The polarisation and angular distribution of the de-excitation radiation can then be described by a Cartesian polarisation matrix $\mathbf{C}$, which is given by (Nienhuis 1980)

$$\mathbf{C} = (\omega_0^4/8\pi^2\varepsilon_0 c^3)\ \mathrm{Tr}_l\, \boldsymbol{\mu}_{lu} \rho_u \boldsymbol{\mu}_{ul} \tag{6}$$

where ω_0 is the angular frequency of the emitted radiation and $\boldsymbol{\mu}_{ul}$ is the electric dipole operator of the atom between the upper (^{1}P) state and the lower (^{1}S) ground state. The matrix $\mathbf{C}$ determines the photon emission in every direction and with any direction of polarisation. The intensity of the emitted radiation with polarisation direction $\hat{\boldsymbol{\varepsilon}}$ is given by

$$I(\hat{\boldsymbol{\varepsilon}}) = \hat{\boldsymbol{\varepsilon}}^* \mathbf{C} \hat{\boldsymbol{\varepsilon}} \tag{7}$$

and the polarisation-independent intensity in a direction $\hat{\boldsymbol{n}}$ is given by

$$I(\hat{\boldsymbol{n}}) = \mathrm{Tr}\,\mathbf{C} - \hat{\boldsymbol{n}}\mathbf{C}\hat{\boldsymbol{n}} \tag{8}$$

i.e. a summation over all possible polarisation directions except for the observation direction. Since the angular momentum $J_u = 1$ for a ^{1}P state, the calculation of the polarisation matrix $\mathbf{C}$ is relatively easy. From the Wigner–Eckhart theorem it follows that

$$\boldsymbol{u}_\sigma^* \mathbf{C} \boldsymbol{u}_{\sigma'} = (\omega_0^4/8\pi^2\varepsilon_0 c^3)\tfrac{1}{3}|\langle 1||\mu||0\rangle|^2 \langle 1\sigma|\rho_u|1\sigma'\rangle \tag{9}$$

where the $\boldsymbol{u}_\sigma$ $(\sigma = -1, 0, 1)$ are the spherical unit vectors. Equation (9) expresses the proportionality between the spherical components of $\mathbf{C}$ and the density matrix elements in the $|J_u M_u\rangle$ basis. In a Cartesian basis the polarisation matrix becomes

$$\mathbf{C} \sim \tfrac{1}{2}\begin{pmatrix} |a_1 - a_{-1}|^2 & -\mathrm{i}(a_1 - a_{-1})(a_1 + a_{-1})^* & 0 \\ \mathrm{i}(a_1 - a_{-1})^*(a_1 + a_{-1}) & |a_1 + a_{-1}|^2 & 0 \\ 0 & 0 & 0 \end{pmatrix}$$

$$= \tfrac{1}{2}\sigma \begin{pmatrix} 1 + P_l \cos 2\gamma & P_l \sin 2\gamma - \mathrm{i}L_\perp & 0 \\ P_l \sin 2\gamma + \mathrm{i}L_\perp & 1 - P_l \cos 2\gamma & 0 \\ 0 & 0 & 0 \end{pmatrix} \tag{10}$$

with $\mu = L_\perp$. Equation (10) expresses the polarisation matrix in terms of parameters directly related to the charge cloud density of the excited ^{1}P state. From equation (4) we have

$$P_l^2 + L_\perp^2 = 1. \tag{11}$$

Equation (10) describes completely the polarisation and angular distribution of the emitted radiation. One can see directly that the light emitted in the scattering plane is linearly polarised and the light emitted perpendicular to the scattering plane in the $+z$ direction is elliptically polarised. With equation (7) we derive the Stokes' parameters P_1, P_2 and P_3 of the elliptically polarised radiation emitted in the $+z$ direction:

$$\begin{aligned} P_1 &= (I(0) - I(\pi/2))/I = P_l \cos 2\gamma \\ P_2 &= (I(\pi/4) - I(3\pi/4))/I = P_l \sin 2\gamma \\ P_3 &= (I(\mathrm{RHC}) - I(\mathrm{LHC}))/I = -\mu \end{aligned} \tag{12}$$

where I is the total light intensity in the $+z$ direction and $I(\theta)$ is the light intensity transmitted through an ideal linear polariser rotated through an angle θ relative to the x axis. For the circular polarisation, we call the light left-hand polarised if the electric vector rotates anticlockwise when looking towards the light source. From equations (12) it follows that the width parameter P_l is equal to the linear polarisation of the radiation emitted in the z direction, i.e. $P_l = (P_1^2 + P_2^2)^{1/2}$. As expected, the emitted light is fully coherent, i.e. $P_1^2 + P_2^2 + P_3^2 = 1$.

In our experiment we do not measure the polarisation of the emitted radiation, but instead the angular distribution of the photons emitted in the scattering plane. From equations (8) and (10) we obtain the angular distribution function

$$I(\varphi_\gamma) \sim 1 - P_l \cos 2(\varphi_\gamma - \gamma) \tag{13}$$

where φ_γ determines the position of the photon detector in the xy scattering plane. We see that an angular correlation experiment is equivalent to a linear polarisation measurement. The alignment angle γ is the direction of minimal photon intensity. Only the absolute value of the transferred angular momentum follows from an angular correlation experiment; the sign of $L_\perp$ can only be determined from a circular polarisation measurement.

2.2. z axis along the direction of the incident electron beam

Theoretical calculations performed in the past have typically chosen the z axis parallel to the incident beam direction $\boldsymbol{K}_\mathrm{a}$ and the y axis perpendicular to the scattering plane.

For this coordinate system, the $m=0$ amplitude is non-zero and the $m=-1$ amplitude is the same as the $m=+1$ amplitude but negative. It is easy to see that if this coordinate system is rotated so that it coincides with that of figure 1, the opposite signs of the ± 1 amplitudes in the original coordinate system cause the $m=0$ amplitude in the new system to vanish. For completeness, the connection between the amplitudes expressed in the two different coordinate systems will now be given.

For a coordinate system with the z axis parallel to $\boldsymbol{K}_a$ and y axis perpendicular to the scattering plane, the pure state is described in an analogous manner to equation (1):

$$|\psi(^1\mathrm{P})\rangle = \sum_M b_M(\theta_e, E)|LM\rangle \tag{14}$$

where $b_{-1}=-b_1$. The connection between the a_M and b_M amplitudes is

$$a_1 = -2^{-1/2}b_0 - \mathrm{i}b_1 \qquad a_{-1} = 2^{-1/2}b_0 - \mathrm{i}b_1. \tag{15}$$

In terms of the b_M amplitudes, the σ, μ and η parameters are

$$\begin{aligned} \sigma &= 2|b_1|^2 + |b_0|^2 \\ \mu &= -(2^{3/2}/\sigma)\,\mathrm{Im}(b_1 b_0^*) \\ \eta &= \tan^{-1}[2^{3/2}\,\mathrm{Re}(b_1 b_0^*)/(2|b_1|^2 - |b_0|^2)]. \end{aligned} \tag{16}$$

2.3. Distorted-wave calculation

We have calculated 2^1P and 3^1P results using four different theoretical models which represent a typical sample of the many different types of distorted-wave (DW) calculations which have been reported in the past. The calculations and their labels are as follows.

(i) MM. This is a standard first-order DW calculation of the Mott and Massey type, where the incident-channel distorted wave is calculated using the ground-state potential and the excited-state distorted wave is calculated using the excited-state potential.

(ii) MB. This is the standard many-body theory type of calculation, where both the initial- and final-channel distorted waves are calculated using the ground-state potential.

(iii) EP. For this calculation, both the initial- and final-channel distorted waves are calculated using the excited-state potential.

(iv) $\frac{1}{3}$-$\frac{2}{3}$. This is the DW model reported in § 3.4 of Madison and Winters (1983). In this model, both the initial- and final-channel distorted waves are calculated using a single potential which is formed as the sum of one third of the ground-state potential plus two thirds of the excited-state potential. This model was found by Madison and Winters (1983) to give the best agreement with the 80 eV experimental data.

For all the above calculations, the initial-state wavefunction was taken to be the 1s wavefunction of the $^1S_0$ ground state and the final-state wavefunction was taken to be the appropriate p state of either the 2^1P or the 3^1P state. First-order exchange was also included in each of the calculations. The MM and MB models are those of Madison (1979). It should be noted that EP is different from the ES model of Madison (1979) in that here we have used the 1s ground-state wavefunction both for the initial-state wavefunction and for calculating the (1s2p) excited-state potential. In Madison's ES model, the 1s excited-state wavefunction of the $(1s2p)^1$P configuration was used to represent the initial-state wavefunction and to calculate the distorting potential. This choice was made at that time in order to satisfy the orthogonality requirement. It is now known that the ground-state wavefunction must be used if one wishes to obtain accurate small-angle differential cross sections. Our experience indicates that having the correct initial- and final-state wavefunctions is more important than satisfying the orthogonality requirement.

3. Experimental method

The electron-photon coincidence experiments were performed with a conventional crossed-beam apparatus, which has been described in an earlier paper (van Linden van den Heuvell *et al* 1982). Briefly, an unselected electron beam was crossed with a thermal helium beam. The scattered electrons were energy analysed and detected in coincidence with the VUV de-excitation photons. The $n = 2$ states were separated from the $n = 3$ states by the energy analyser. The energy resolution was not sufficient to separate the 3^1S, 3^1P and 3^1D states, but for the incident electron energies considered ($\geqslant 50$ eV) the contribution of the 3^1D state to the coincidence signal (via cascade to the 2^1P state) is negligible (van Linden van den Heuvell *et al* 1983).

The electron gun was based upon the design of Harting and Burrows (1970). To obtain a low-divergent beam, a Pierce extraction system was used with a stripper electrode. We calculated the electron trajectories in this gun with a ray tracing program to gain some insight into its focusing properties. For a realistic setting of the lens element voltages we calculated a beam current of 0.45 μA, which was in agreement with the experimental value. The calculated beam diameter and divergence were 2 mm and 0.03 rad respectively. Throughout the experiments we used a beam current of 0.5-2.5 μA in the energy range 50-80 eV. A Faraday cup was located behind the scattering centre to collect the unscattered electrons.

The atomic beam was generated by effusing helium from a chamber at a relatively high pressure (approximately 40 Pa = 0.3 Torr) through a single needle with a length of 10 mm and an inner diameter of 0.4 mm. We estimated the helium density at the scattering centre to be approximately 8×10^{17} m^{-3}. The scattered electrons were energy selected by a hemispherical electron analyser. Two three-element lenses focused the scattered electrons onto the virtual entrance slit of the hemispheres. After passage through the hemispheres, the energy-selected electrons were focused onto the cathode of an electron multiplier (Hamamatsu R515). The maximum acceptance solid angle of the electron analyser was estimated to be 4×10^{-3} sr.

The VUV de-excitation photons were detected by a Mullard X919BL channel electron multiplier, which is insensitive to the polarisation of the photons. To prevent electrons, ions and metastable atoms from being detected, three suitably biased grids and a thin tin foil were mounted in front of the channeltron housing. The acceptance solid angle subtended by the channeltron at the scattering centre was 0.27 sr. Both the electron and photon detectors could be rotated independently in the horizontal plane around the scattering centre; the channeltron was also rotatable in the vertical plane. For the electron analyser we had an angular range from 30 to about 100° and for the photon detector from 46 to 136°.

The whole experimental set-up was mounted inside a large vacuum tank pumped by two oil diffusion pumps with a pumping speed of 2.5 m^3 s^{-1} each. To prevent oil vapour from entering the apparatus, the two pumps were baffled with liquid nitrogen traps. Under typical operating conditions the background pressure in the vacuum tank was about 4.6×10^{-5} Pa (3.5×10^{-7} Torr), which dropped to 9.3×10^{-7} Pa (7×10^{-9} Torr) without any inlet of gas. To reduce the influence of magnetic fields, the whole apparatus was surrounded by three pairs of rectangular Helmholtz coils. The residual magnetic field at and near the scattering centre was measured to be less than a few μT. This field had a negligible effect on the electron trajectories in the apparatus.

The signal processing followed conventional lines. The pulses from the electron multiplier and channeltron were fed into snap-off discriminators (Elscint STD 1 and 2), which have a minimum detection threshold of 1 mV. The electron pulses were used to start the ramp of a time-to-amplitude converter (TAC; Ortec 467). The photon pulses stopped the TAC after a suitable delay (typically 300 ns). The output pulses from the TAC were then analysed according to their amplitudes by a multichannel analyser (MCA; Tracor 1700).

In order to determine the anisotropy parameters for a certain energy and scattering angle, a series of time spectra were measured for ten different photon angles, all in the scattering plane. After subtracting the background from the area under the peak, the total number of coincidences in each time spectrum was determined. To correct for small drifts in electron beam current and helium pressure, the total number of coincidences in each spectrum was normalised to the total number of true TAC starts counted in the same time. Finally, by fitting equation (13) to the measured angular distribution of coincident photons, the anisotropy parameters P_l and γ were determined for each energy and electron scattering angle considered.

The following sources of systematic error were considered. Firstly, the angular distribution function (equation (13)) was corrected for the finite acceptance angle of the photon detector. Assuming that the detector efficiency is constant over the aperture, the integration of equation (13) over the acceptance angle can be carried out exactly (this is simply done by rotating the coordinate system so that the z axis becomes parallel to the symmetry axis of the channeltron). The corrected angular distribution function then reads

$$I_c(\varphi_\gamma) = [\kappa I(\varphi_\gamma) + \tfrac{2}{3}(1-\kappa)]\Delta\Omega_\gamma \qquad (17)$$

where

$$\kappa = (1 - \Delta\Omega_\gamma/2\pi)(1 - \Delta\Omega_\gamma/4\pi) \qquad (18)$$

and $\Delta\Omega_\gamma$ is the acceptance angle of the channeltron. In the present experiment we had $\kappa = 0.936$. Secondly, the absorption and re-emission of resonant photons by ground-state atoms can have a significant effect on the measured anisotropy parameters. We determined the influence of this effect by measuring the anisotropy parameters P_l and γ as a function of the helium inlet pressure. This is a time-consuming task and was therefore performed only for 2^1P excitation at an energy of 60 eV and an electron scattering angle $\theta_e = 30°$. The results are shown in figure 3. The alignment angle γ appears not to be seriously affected by radiation trapping, while the linear polarisation P_l decreases steadily for inlet pressures greater than 28 Pa. These findings are in agreement with those of Hollywood *et al* (1979), who concluded that the position of the minimum of the angular correlation curve did not change while the amplitude decreased with increasing inlet pressure. Our subsequent experiments were performed with a helium inlet pressure well below 28 Pa.

Another systematic error may occur as a result of a time variation of the channeltron efficiency. This error was eliminated to first order by scanning the photon angular range back and forth in each run. We also checked the pulse height distribution of the channeltron before and after each run. Furthermore, the photon count rate was

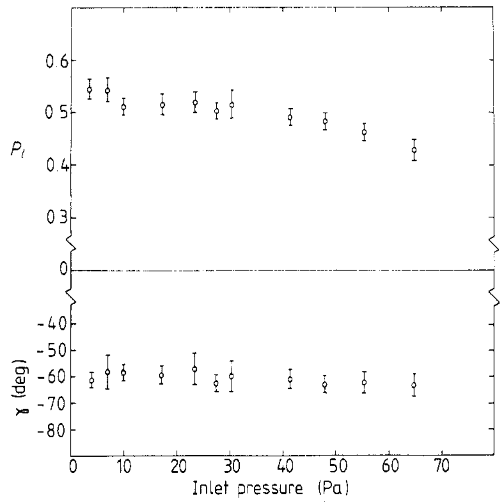

Figure 3. The anisotropy parameters P_l and γ as a function of the helium inlet pressure for 2^1P excitation at an energy of 60 eV and an electron scattering angle $\theta_e = 30°$.

constantly kept below $2\times10^4\,s^{-1}$. Finally, we calibrated the angular position of the photon detector before each run and the maximum of the photon intensity was verified to be at $\theta_\gamma = 90°$.

The sinusoidal fits to the measured angular distributions were of a high quality. We were therefore convinced that the most important sources of systematic errors had been eliminated satisfactorily.

4. Results and conclusions

We measured the P_l and γ parameters for 2^1P and 3^1P excitation at different incident electron energies. In table 1 our values of P_l and γ are given for 2^1P excitation as a function of the scattering angle at incident electron energies of 50, 60 and 80 eV. Table 2 contains corresponding results for 3^1P excitation at incident electron energies of 50 and 80 eV. In both tables, the angular momentum transfer $L_\perp$ calculated from equation (11) is also given. Although it is not possible to obtain the sign of $L_\perp$ from an angular correlation experiment, we assumed that $L_\perp$ is positive for small scattering angles (cf Standage and Kleinpoppen 1976, Williams 1983, Madison *et al* 1986). The angular position where P_l is equal to or near unity is interpreted as the position where a sign change in $L_\perp$ occurs. For larger angles, $L_\perp$ becomes negative. Thus we want to revoke our earlier conclusions concerning 2^1P excitation at 50 and 60 eV (Beijers *et al* 1984). As pointed out by Andersen *et al* (1985), the angular correlation pattern of the coincident photons does not change much in the region where P_l is near unity. Thus the observation of a zero crossing of $L_\perp$ in an angular correlation experiment is extremely difficult. Presented in terms of the P_l and γ parameters, our results do indicate a sign reversal of $L_\perp$ for all energies measured for both 2^1P and 3^1P excitation. Direct circular polarisation measurements as a function of the electron scattering angle have been performed recently for 2^1P excitation (Khakoo *et al* 1985) and 3^1P excitation (Ibraheim *et al* 1985, Beijers *et al* 1986) in the intermediate-energy range. Both

Table 1. Experimental values of the target parameters $L_\perp$, P_l and γ for the 2^1P state as a function of the electron scattering angle θ_e for incident electron energies of 80, 60 and 50 eV.

	θ_e (deg)	$L_\perp$	$P_l = (1-\mu^2)^{1/2}$	γ (deg)
$E = 80$ eV				
	25	0.72 ± 0.01	0.694 ± 0.010	-63.0 ± 1.1
	40	0.870 ± 0.044	0.493 ± 0.078	-0.5 ± 3.6
	50	0.498 ± 0.070	0.867 ± 0.040	5.6 ± 1.1
	60	0.02 ± 0.10	1.000 ± 0.002	8.1 ± 1.1
	70	-0.60 ± 0.10	0.800 ± 0.075	12.6 ± 3.0
$E = 60$ eV				
	30	0.857 ± 0.005	0.515 ± 0.008	-60.6 ± 1.6
	31.5	0.876 ± 0.004	0.482 ± 0.007	-60.5 ± 1.3
	40	0.971 ± 0.012	0.239 ± 0.049	-30.2 ± 6.5
	50	0.715 ± 0.040	0.699 ± 0.041	7.1 ± 1.8
	55	0.39 ± 0.15	0.921 ± 0.064	9.8 ± 2.1
	57	0.34 ± 0.12	0.940 ± 0.043	9.4 ± 1.2
	60	-0.426 ± 0.054	0.905 ± 0.025	11.2 ± 1.1
	65	-0.33 ± 0.10	0.944 ± 0.035	12.5 ± 1.6
	70	-0.549 ± 0.080	0.836 ± 0.053	18.3 ± 2.6
	80	-0.77 ± 0.14	0.638 ± 0.17	20.1 ± 6.3
	90	-0.788 ± 0.082	0.616 ± 0.10	29.0 ± 9.7
	100	-0.707 ± 0.075	0.707 ± 0.075	24.4 ± 18.3
$E = 50$ eV				
	30	0.702 ± 0.006	0.713 ± 0.006	-54.9 ± 0.9
	31.5	0.829 ± 0.007	0.559 ± 0.010	-57.1 ± 2.0
	40	0.985 ± 0.007	0.174 ± 0.039	-22.4 ± 10.9
	50	0.843 ± 0.023	0.538 ± 0.036	8.6 ± 1.7
	60	0.608 ± 0.053	0.794 ± 0.041	13.4 ± 1.3
	65	0.620 ± 0.051	0.785 ± 0.040	20.5 ± 2.2
	67.5	0.48 ± 0.18	0.877 ± 0.098	19.1 ± 4.1
	70	-0.592 ± 0.063	0.806 ± 0.046	17.6 ± 1.8
	75	-0.635 ± 0.066	0.773 ± 0.054	24.8 ± 3.7
	80	-0.636 ± 0.088	0.772 ± 0.073	28.7 ± 5.7
	90	-0.636 ± 0.077	0.772 ± 0.063	29.8 ± 6.3

experiments clearly show the occurrence of a sign reversal in $L_\perp$ for all energies measured, thus solving this obstinate problem conclusively.

In figures 4-8 the present experimental $L_\perp$, P_l and γ parameters are plotted as a function of the electron scattering angle for 2^1P and 3^1P excitation together with the results of several other experimental groups and the results of the theoretical calculations. The experimental alignment and orientation parameters show the same characteristics both for 2^1P and 3^1P excitation and for all energies measured. At $\theta_e = 0$ and 180°, $L_\perp = 0$, $\gamma = 0$ and $P_l = 1$ from symmetry considerations. For small scattering angles, the excited-electron cloud is rotated away from the scattered electron ($\gamma < 0$) and γ reaches a minimum around $\theta_e = 30°$. The charge cloud then rotates back through the primary beam direction and γ becomes positive. At larger scattering angles, γ reaches a maximum and returns again to the primary beam axis. For 60 and 80 eV, γ again becomes negative for the largest scattering angles measured.

The different theoretical models predict very different behaviours for γ. The only model to give the qualitative behaviour exhibited by the experimental data for all energies is the EP model. The EP model is also in reasonably good quantitative

Table 2. Experimental values of the target parameters $L_\perp$, P_l and γ for the 3^1P state as a function of the electron scattering angle θ_e for incident electron energies of 80 and 50 eV.

	θ_e (deg)	$L_\perp$	$P_l = (1-\mu^2)^{1/2}$	γ (deg)
$E = 80$ eV				
	25	0.755 ± 0.019	0.656 ± 0.022	-56.0 ± 3.9
	30	0.866 ± 0.008	0.500 ± 0.013	-51.9 ± 2.9
	35	0.948 ± 0.008	0.320 ± 0.024	-28.2 ± 4.7
	40	0.956 ± 0.013	0.293 ± 0.042	-1.4 ± 3.4
	45	0.712 ± 0.051	0.702 ± 0.052	6.6 ± 1.9
	50	0.661 ± 0.085	0.750 ± 0.075	8.4 ± 2.4
	55	0.640 ± 0.084	0.768 ± 0.070	10.4 ± 2.2
	60	0.670 ± 0.054	0.742 ± 0.049	13.5 ± 2.0
	65	0.24 ± 0.36	0.971 ± 0.089	13.2 ± 2.2
	70	-0.829 ± 0.035	0.559 ± 0.052	18.4 ± 3.4
	75	-0.871 ± 0.033	0.491 ± 0.059	23.8 ± 6.3
$E = 50$ eV				
	25	0.708 ± 0.017	0.706 ± 0.017	-44.6 ± 2.4
	30	0.753 ± 0.011	0.658 ± 0.013	-45.8 ± 1.9
	35	0.867 ± 0.012	0.498 ± 0.021	-43.1 ± 4.0
	40	0.954 ± 0.009	0.299 ± 0.028	-34.4 ± 7.4
	45	0.912 ± 0.034	0.410 ± 0.076	-2.7 ± 3.6
	50	0.903 ± 0.025	0.430 ± 0.053	14.0 ± 4.6
	55	0.800 ± 0.056	0.600 ± 0.075	16.9 ± 4.4
	60	0.60 ± 0.11	0.800 ± 0.083	16.9 ± 3.5
	62.5	0.674 ± 0.060	0.739 ± 0.055	18.8 ± 2.8
	65	0.43 ± 0.37	0.903 ± 0.18	19.8 ± 2.2
	67.5	-0.729 ± 0.045	0.685 ± 0.048	24.0 ± 3.4
	70	-0.56 ± 0.12	0.828 ± 0.081	22.3 ± 4.1
	75	-0.717 ± 0.061	0.697 ± 0.063	29.4 ± 5.6
	80	-0.59 ± 0.13	0.807 ± 0.095	25.8 ± 5.6
	85	-0.63 ± 0.12	0.777 ± 0.097	29.6 ± 7.4

agreement with the data for scattering angles out to about 60°. The $\frac{1}{3}$-$\frac{2}{3}$ model, which had previously given the best agreement for the λ and χ parameters and the differential cross section at 80 eV, also predicts the experimentally observed behaviour for γ at 80 eV but not for the lower energies. If one views the scattering plane from the positive z axis, the MM and MB models predict that the charge cloud will rotate clockwise, with the forward lobe initially entering the fourth quadrant and the backward lobe initially in the second quadrant. However, instead of stopping and reversing the direction of rotation as was observed experimentally, MM and MB predict a continued clockwise rotation with the forward lobe going into the third quadrant and the backward lobe entering the first quadrant. This quadrant change produces the π discontinuity in γ seen in the figures. For MM and MB (and the lower-energy $\frac{1}{3}$-$\frac{2}{3}$ models), the clockwise rotation continues until the initially backward lobe reaches the fourth quadrant, at which time the rotation slowly reverses and the charge distribution finally aligns with the incident beam direction for backward scattering. From this discussion it should be noted that even though all models predict γ to be zero for $\theta_e = 180°$, the experimental data and the EP model predict that this results from the initially forward lobe remaining forward for all scattering angles, while the MM and MB models predict that the initially forward lobe rotates backwards for large-angle scattering. The value of looking at the γ parameter now becomes clear. At 50 and 60 eV, the EP and $\frac{1}{3}$-$\frac{2}{3}$ models give almost

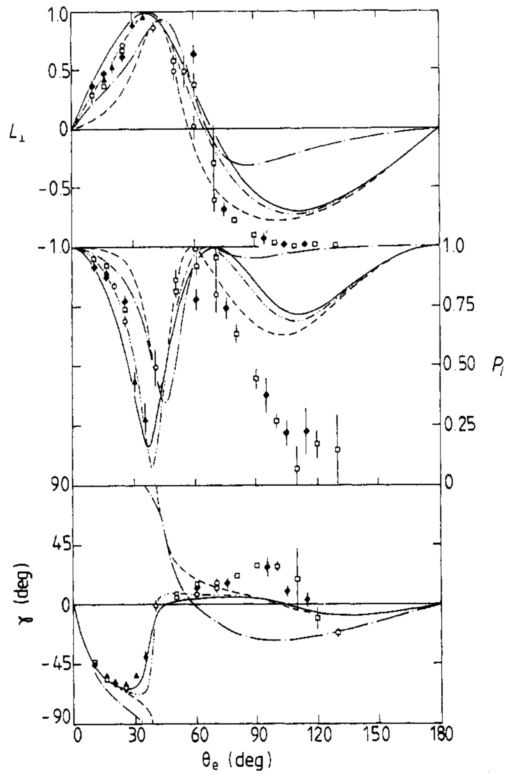

Figure 4. The anisotropy parameters $L_\perp$, P_l and γ as a function of the electron scattering angle for 2^1P excitation at an incident electron energy of 80 eV. Experimental: ○, present results; ▲, Eminyan *et al* (1974); ◆, Slevin *et al* (1980); □, Hollywood *et al* (1979) at 81.2 eV. Theoretical: — · —, MM model; - - -, MB model; ——, EP model; — · · —, $\frac{1}{3}$-$\frac{2}{3}$ model.

the same γ parameters, except for a very narrow angular range where EP predicts a reversal in the direction of rotation and $\frac{1}{3}$-$\frac{2}{3}$ predicts a very rapid continuous clockwise rotation. An examination of the λ and χ parameters gives no indication that these two models predict different types of physical behaviour in this angular region.

The angular momentum transfer $L_\perp$ also shows the same structure for every measured energy, both for 2^1P and 3^1P. At small scattering angles, $L_\perp$ is positive and reaches a maximum around $\theta_e = 40°$. At this maximum the emitted light perpendicular to the scattering plane is almost fully left-hand circularly polarised. For increasing θ_e, $L_\perp$ decreases and changes sign at some intermediate scattering angle. The emitted light becomes right-hand circularly polarised and $L_\perp$ becomes negative. It then reaches a minimum and returns to zero for $\theta_e = 180°$. Madison *et al* (1986) noted that theoretical calculations predict that the crossover point from positive to negative for $L_\perp$ moves to smaller angles with increasing incident electron energy. While different experiments give a range of crossover points, the general trend seems to support the theoretical prediction. In terms of agreement between experiment and theory for $L_\perp$, MM is generally bad. The EP and $\frac{1}{3}$-$\frac{2}{3}$ models give the qualitative shape of $L_\perp$ and are in fairly good quantitative agreement at small angles, with $\frac{1}{3}$-$\frac{2}{3}$ being slightly better.

For some time, the sign change of $L_\perp$ has been interpreted in terms of a grazing-incidence model, with attractive and repulsive forces. Classically, an attractive interac-

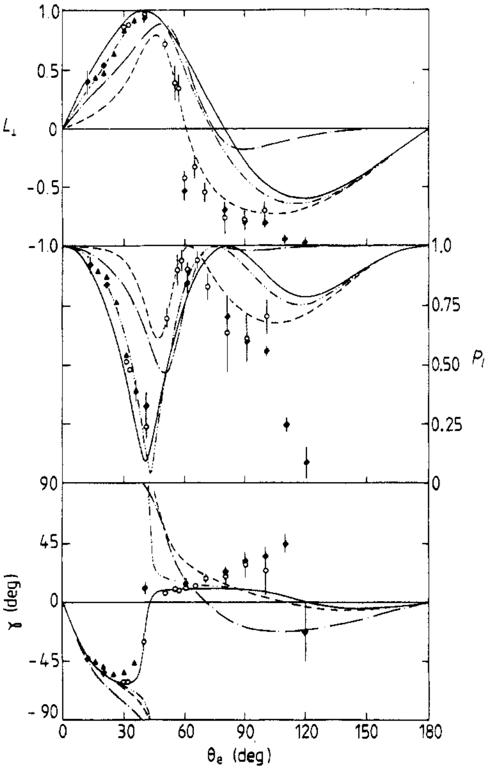

Figure 5. As figure 4 but for 2^1P excitation at 60 eV incident electron energy.

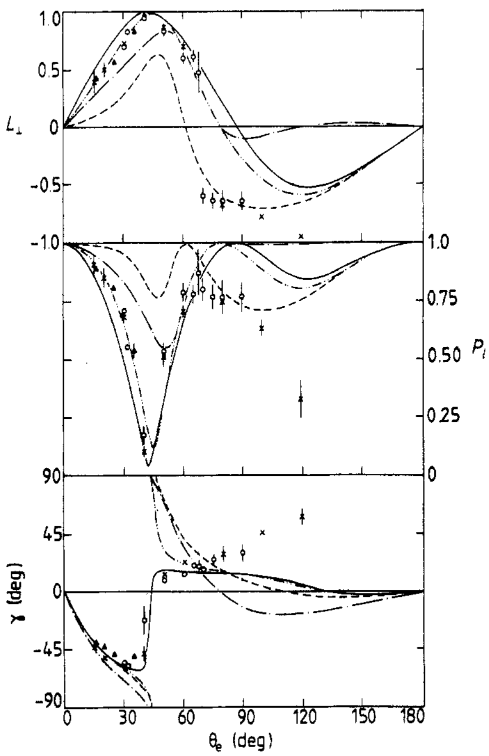

Figure 6. As figure 4 but for 2^1P excitation at 50 eV incident electron energy. Experimental data: ×, McAdams *et al* (1980) at 51.2 eV.

tion leads to a positive $L_\perp$ and a repulsive interaction to a negative $L_\perp$. At small scattering angles, the electron-atom interaction was believed to be dominated by attractive polarisation forces, while at larger scattering angles the electron-electron repulsion was assumed to dominate the interaction. However, Madison *et al* (1986) pointed out that this reasoning is incorrect. They showed that the characteristic shape of $L_\perp$ is not determined by the attractive polarisation potential and the repulsive electron-electron potential. The effective atomic potential is attractive for all radii and is dominated by the nucleus. The nuclear attraction alone provides the characteristic shape for $L_\perp$. A greater understanding of the sign of $L_\perp$ is gained through a formal Born series expansion of the scattering amplitudes (Madison and Winters 1981). They show that the lowest-order term of the angular momentum transfer $L_\perp$ is proportional to the projectile charge q, whereas the next-highest term is proportional to q^2. At small scattering angles the first-order term is dominant; this results in a sign reversal when going from e^- to e^+ scattering, and at large scattering angles the second-order term dominates with no charge sign dependence. For e^- scattering the angular momentum transfer $L_\perp$ vanishes when the first- and second-order terms are equal.

In conclusion, we have measured the P_l and γ parameters for 50–80 eV excitation of both the 2^1P and 3^1P states of helium. Of the theoretical models considered, only the EP model gives qualitative agreement for both states and all three energies. The MB and MM models predict an incorrect behaviour for the rotation of the charge cloud.

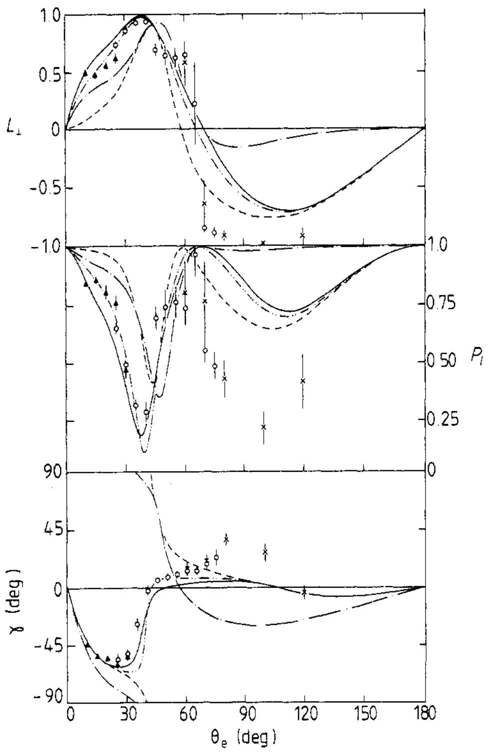

Figure 7. As figure 4 but for 3^1P excitation at 80 eV incident electron energy. Experimental data: ○, present results; ▲, Eminyan *et al* (1975); ×, McAdams and Williams (1982) at 81.2 eV.

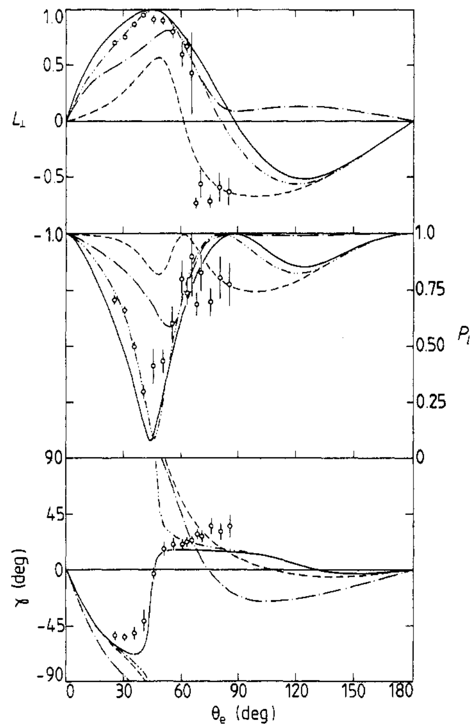

Figure 8. As figure 7 but for 3^1P excitation at 50 eV incident electron energy.

The $\frac{1}{3}$-$\frac{2}{3}$ model was designed for 80 eV, and while it gives a somewhat better agreement than EP for $L_\perp$ at all energies and both states, it predicts an incorrect behaviour for the γ parameter at 50 and 60 eV. The value of the $\frac{1}{3}$-$\frac{2}{3}$ model for higher energies has yet to be determined. We would conclude (as did Madison and Winters (1983)) that for best agreement between theory and experiment, first-order distorted-wave calculations should be performed using the excited-state potential for distorting both the initial- and final-state electrons. The common practice of using the ground-state potential for both channels leads to incorrect physical behaviour for the γ parameter.

Acknowledgments

The authors would like to thank N Andersen and I V Hertel for helpful discussions, M A M de Jong for performing the pressure-dependent measurements and J van der Weg for technical support. This work was performed as part of the research programme of the Stichting voor Fundamenteel Onderzoek der Materie (FOM) with financial support from the Nederlandse Organisatie voor Zuiver-Wetenschappelijk Onderzoek (ZWO) and from the NSF under grant PHY-8310644.

References

Andersen N, Gallagher J W and Hertel I V 1985 *Proc. 14th Int. Conf. on Physics of Electronic and Atomic Collisions (Palo Alto) 1985* ed D C Lorents, W E Meyerhof and J R Peterson (Amsterdam: North-Holland) Invited papers pp 57-76

Beijers J P M, van den Brink J P, van Eck J and Heideman H G M 1986 *J. Phys. B: At. Mol. Phys.* **19** L581-5

Beijers J P M, van Eck J and Heideman H G M 1984 *J. Phys. B: At. Mol. Phys.* **17** L265-9

Blum K and Kleinpoppen H 1975 *J. Phys. B: At. Mol. Phys.* **8** 922-5

—— 1979 *Phys. Rep.* **52** 203-61

Crowe A, Nogueira J C and Liew Y C 1983 *J. Phys. B: At. Mol. Phys.* **16** 481-9

Danjo A, Koike T, Kani K, Sugahara H, Takahashi A and Nishimura H 1985 *J. Phys. B: At. Mol. Phys.* **18** L595-600

Eminyan M, MacAdam K B, Slevin J and Kleinpoppen H 1973 *Phys. Rev. Lett.* **31** 576-9

—— 1974 *J. Phys. B: At. Mol. Phys.* **7** 1519-42

Eminyan M, MacAdam K B, Slevin J, Standage M C and Kleinpoppen H 1975 *J. Phys. B: At. Mol. Phys.* **8** 2058-66

Fano U and Macek J H 1973 *Rev. Mod. Phys.* **45** 553-73

Fon W C, Berrington K A and Kingston A E 1980 *J. Phys. B: At. Mol. Phys.* **13** 2309-25

Harting E and Burrows K M 1970 *Rev. Sci. Instrum.* **41** 97-101

Hermann H W and Hertel I V 1982 *Comment. At. Mol. Phys.* **12** 61-84

Hollywood M T, Crowe A and Williams J F 1979 *J. Phys. B: At. Mol. Phys.* **12** 819-34

Ibraheim K S, Beyer H J and Kleinpoppen H 1985 *Proc. 2nd Eur. Conf. on Atomic and Molecular Physics (Amsterdam) 1985* ed A E de Vries and M J van der Wiel (Amsterdam: Free University Press) p 298

Khakoo M A, Forand L, Becker K and McConkey J W 1985 *Proc. 14th Int. Conf. on Physics of Electronic and Atomic Collisions (Palo Alto) 1985* (Amsterdam: North-Holland) Abstracts p 111

King S J, Neill P A and Crowe A 1985 *J. Phys. B: At. Mol. Phys.* **18** L589-94

Macek J and Jaecks D H 1971 *Phys. Rev.* A **4** 1288-300

Madison D H 1979 *J. Phys. B: At. Mol. Phys.* **12** 3399-414

—— 1984 *Phys. Rev. Lett.* **53** 42-5

Madison D H, Csanak G and Cartwright D C 1986 *J. Phys. B: At. Mol. Phys.* **19** 3361-6

Madison D H and Winters K H 1981 *Phys. Rev. Lett.* **47** 1885-7

—— 1983 *J. Phys. B: At. Mol. Phys.* **16** 4437-50

McAdams R, Hollywood M T, Crowe A and Williams J F 1980 *J. Phys. B: At. Mol. Phys.* **13** 3691-701

McAdams R and Williams J F 1982 *J. Phys. B: At. Mol. Phys.* **15** L247-51

Neill P A and Crowe A 1984 *J. Phys. B: At. Mol. Phys.* **17** L791-5

Nienhuis G 1980 *Coherence and Correlation in Atomic Collisions* ed H Kleinpoppen and J Williams (New York: Plenum) pp 121-32

Slevin J 1984 *Rep. Prog. Phys.* **47** 461-512

Slevin J, Porter H Q, Eminyan M, Delfrance A and Vassilev G 1980 *J. Phys. B: At. Mol. Phys.* **13** 3009-21

Standage M C and Kleinpoppen H 1976 *Phys. Rev. Lett.* **36** 577-80

Steph N C and Golden D E 1980 *Phys. Rev.* A **21** 759-70

van Linden van den Heuvell H B, Nienhuis G, van Eck J and Heideman H G M 1981 *J. Phys. B: At. Mol. Phys.* **14** 2667-76

van Linden van den Heuvell H B, van Eck J and Heideman H G M 1982 *J. Phys. B: At. Mol. Phys.* **15** 3517-33

van Linden van den Heuvell H B, van Gasteren E M, van Eck J and Heideman H G M 1983 *J. Phys. B: At. Mol. Phys.* **16** 1619-31

Walters H R J 1984 *Phys. Rep.* **116** 1-102

Williams J F 1983 *Proc. 13th Int. Conf. Physics of Electronic and Atomic Collisions (Berlin) 1983* ed J Eichler *et al* (Amsterdam: North-Holland) Abstracts p 132